TECHNICAL REPORT R-18

SEVERAL METHODS FOR AERODYNAMIC REDUCTION OF STATIC-PRESSURE SENSING ERRORS FOR AIRCRAFT AT SUBSONIC, NEAR-SONIC, AND LOW SUPERSONIC SPEEDS

By VIRGIL S. RITCHIE

Langley Research Center
Langley Field, Va.

TECHNICAL REPORT R–18

SEVERAL METHODS FOR AERODYNAMIC REDUCTION OF STATIC-PRESSURE SENSING ERRORS FOR AIRCRAFT AT SUBSONIC, NEAR-SONIC, AND LOW SUPERSONIC SPEEDS

By VIRGIL S. RITCHIE

SUMMARY

Several methods for aerodynamic reduction of errors in sensing static pressures at subsonic, near-sonic, and low supersonic speeds were investigated by tests of error-reduction probes ahead of aircraft models in transonic wind tunnels. The tests were conducted at Mach numbers from 0.4 to 1.2 with Reynolds numbers (per foot) from 2.3×10^6 to 4.2×10^6 for angles of attack from 0° to 8°.

The principal static-pressure error investigated was that due to position of pressure-sensing device ahead of airplane fuselage or missile nose; a suitable means for estimating this error was provided by combined flight and wind-tunnel data. A method of error compensation by use of probe-surface induced pressures is described and results of tests to verify the method are included. Other investigated errors included those associated with bow-wave passage at low supersonic speeds and with angle of attack. Simple methods for combining the aerodynamic reduction of these errors with aerodynamic compensation for position error are described and experimental results that validate these methods are presented.

Results of the present investigation indicated that static-pressure probes of simple design can be used to compensate aerodynamically for position errors at Mach numbers up to about 1.0 with resultant static-pressure errors of less than 0.5 percent—equivalent to altitude errors of about 100 feet. The results also showed that probes of appropriate design can aerodynamically reduce combined errors due to position of sensing device and bow-wave passage, or to position and angle of attack, to resultant errors of less than 0.5 percent.

INTRODUCTION

The advances of aircraft speed into and through the transonic range, with attendant increases in flight-safety problems, have accentuated the need for improved accuracy in determining the flight parameters of altitude, airspeed, and Mach number. This needed accuracy is largely dependent upon the correct measurement of free-stream static pressure. The accurate determination of this pressure at transonic speeds is difficult, however, principally because of pressure sensing errors associated with the static-pressure probe and its attitude and position in the disturbed field of flow near the aircraft. The magnitude of such errors, as indicated by flight data for conventional nose-boom airspeed installations ahead of various aircraft (ref. 1), is sometimes larger than 10 percent of the free-stream static pressure at transonic speeds (fig. 1); this is equivalent to altitude errors of several thousand feet and to Mach number errors of approximately 10 percent at near-sonic speeds. The necessity for reducing errors of this magnitude has recently been emphasized in connection with flight-safety problems associated with air-traffic control (where vertical separation of aircraft is necessary for avoidance of midair collisions) and with the accurate performance of pressure-sensitive automatic control systems of airplanes and aerodynamic missiles.

A static-pressure-measurement accuracy equivalent to a pressure-altitude accuracy of about 100 feet appears desirable from considerations of flying safety at both subsonic and supersonic speeds. Figure 2 shows that this pressure-altitude accuracy corresponds for standard atmospheric conditions (ref. 2) to about 0.5 percent of the static pressure. The attainment of this accuracy by use of a conventional nose-boom pressure installation ahead of a typical aircraft would

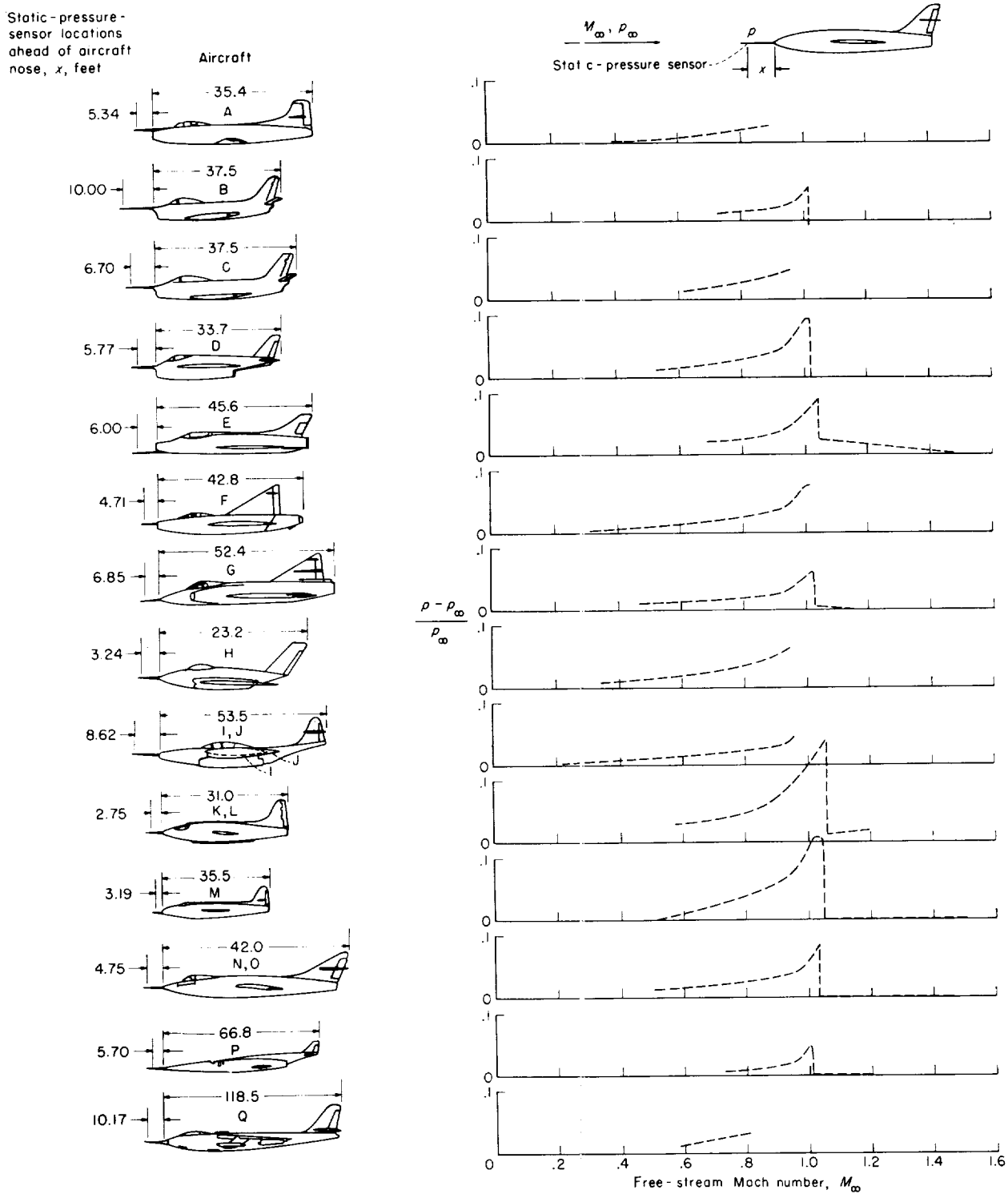

FIGURE 1.—Static-pressure errors due to position of sensor ahead of various aircraft at subsonic and transonic speeds. Data from reference 1; dimensions are in feet.

necessitate the use of an impractically long boom extending several fuselage diameters ahead of the aircraft nose. The use of a boom of any practical length would position the pressure-sensing orifices

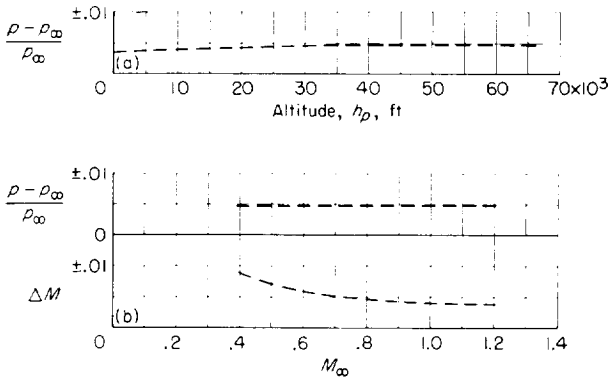

(a) Variation of static-pressure error with altitude.
(b) Variation of static-pressure and Mach number errors with Mach number. 36,000 feet $< h_p <$ 65,800 feet.

FIGURE 2.—Static-pressure and Mach number errors corresponding to pressure-altitude error of 100 feet for standard atmospheric conditions.

in a field of increasing disturbance near the aircraft where pressures sensed by a conventional probe would require correction for position error. This correction can be applied by use of electromechanical systems (ref. 3), but the complexity of such systems emphasizes the desirability of utilizing simpler error-compensation devices based on aerodynamic instead of electrical and mechanical principles. Some early work on aerodynamic compensation of position error was described in reference 4 and more recent investigations were reported in references 5 to 8; these previous attempts employed the base pressures of bluff bodies for error compensation.

The present research was undertaken to investigate an aerodynamic-compensation method based upon the simple aerodynamic concept of using induced pressures lower than free stream at surfaces of bodies of revolution to compensate for the pressures higher than free stream at selected positions ahead of aircraft noses. This investigation involved wind-tunnel tests for experimentally checking the performances of probes designed to compensate aerodynamically for the position error ahead of several aircraft models at subsonic speeds as well as probes designed to provide free-stream static pressure at low supersonic speeds and aerodynamic compensation for position error at subsonic speeds. Probes designed to provide aerodynamic reduction of combined errors due to sensing-device position and angle of attack were also tested. The tests were conducted in transonic wind tunnels at the Langley Research Center at Mach numbers from 0.4 to 1.2, Reynolds numbers (per foot) from 2.3×10^6 to 4.2×10^6, and angles of attack from 0° to 8°.

SYMBOLS

d	maximum diameter of probe
D	maximum diameter of body or fuselage
f	fineness ratio of body or fuselage
h_p	pressure altitude
l	effective length of body or fuselage (twice the axial distance from nose to maximum-diameter station)
M	local Mach number
M_∞	free-stream Mach number
ΔM	Mach number error
p	local static pressure or pressure sensed by probe
p_{TC}	tunnel-calibration reference pressure in tank surrounding slotted test section
p_∞	free-stream static pressure
p_t	stagnation or total pressure
r	local radius of body
R	Reynolds number or radius of circular-arc support strut
U	free-stream velocity
x	axial distance from nose of aircraft or model
x'	axial distance from tip of probe nose
y'	distance from center line to surface of probe
α	angle of attack
θ	circumferential location of orifice from the bottom of the probe
μ	viscosity of air
ρ	mass density of air (free stream)

Subscripts:

des	design value
meas	measured value
x	value at position x ahead of aircraft or model nose
1, 2, 3, 4	axial locations for probe orifices

PRINCIPLES OF ERROR-REDUCTION METHODS

COMPENSATION FOR POSITION ERROR

The present method of obtaining an accurate indication of free-stream static pressure for aircraft or missiles depends on the approximate cancellation of two pressure characteristics, as illustrated in figure 3. The first characteristic, the axial gradient of static pressure ahead of a body (fig. 3(a)), arises from deceleration of the flow ahead of the

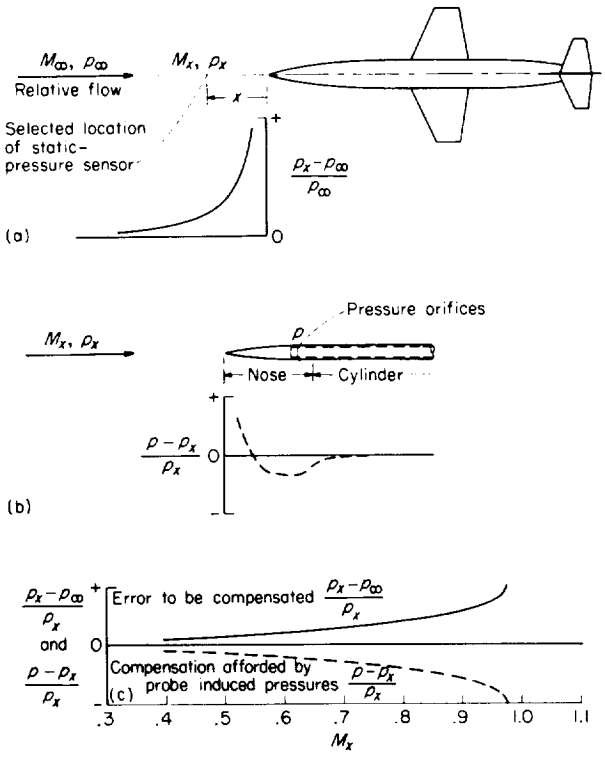

(a) Static-pressure error due to sensor position in subsonic flow ahead of aircraft for a particular Mach number.
(b) Probe induced pressures suitable for use in aerodynamic compensation for position error for a particular Mach number.
(c) Typical variation with Mach number of error to be compensated and of approximate compensation afforded by probe induced pressures.

FIGURE 3.—Illustration of present method involving the use of probe-surface induced pressures for aerodynamic compensation for static-pressure error due to sensor position ahead of aircraft at subsonic and near-sonic speeds.

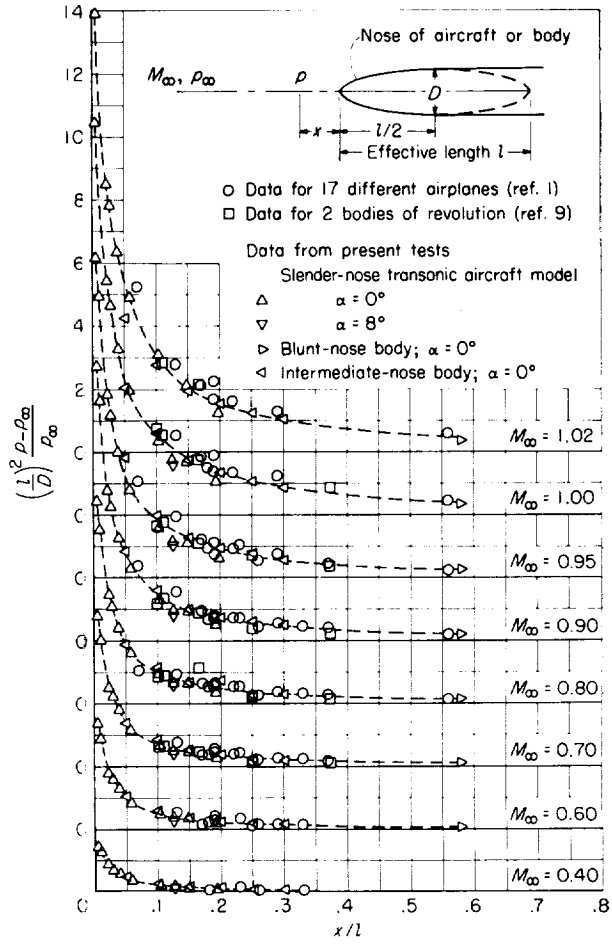

FIGURE 4.—Variation of position-error parameter $(l/D)^2 \frac{p - p_\infty}{p_\infty}$ with distance ahead of aircraft or aerodynamic bodies at Mach numbers from 0.40 to 1.02.

body at subsonic speeds. It would be desirable to know these gradients precisely for any configuration on which it is necessary to install a static-pressure sensor. However, if such measurements are lacking, these pressure gradients and their variation with Mach number may be estimated from a generalized chart (fig. 4). This chart combines data from references 1 and 9 as well as data from the present investigation for configurations similar to airplane fuselages and missile bodies. Similar charts could be developed for locations ahead of aircraft wings by use of such data as are given in references 10 and 11.

The second pressure characteristic is that of the induced pressure on bodies, generally bodies of revolution. (See fig. 3(b).) It is demonstrated in this report that orifices can be located on such bodies at points where the magnitude and variation with Mach number of surface pressures is opposite to that existing in the field ahead of a fuselage (fig. 3(c)). For best results, then, a probe should be shaped to produce induced pressures approximately opposite to the errors due to position when a comparison is made on the basis of the local Mach number at the station of measurement (fig. 3(c)). Sufficient data are available on body-of-revolution pressure distributions to provide a wide range of selection of induced-pressure level. (See, for example, refs. 12 to 17.) Some of these data which have been used for the design of probes used in the present investigation are shown in figure 5.

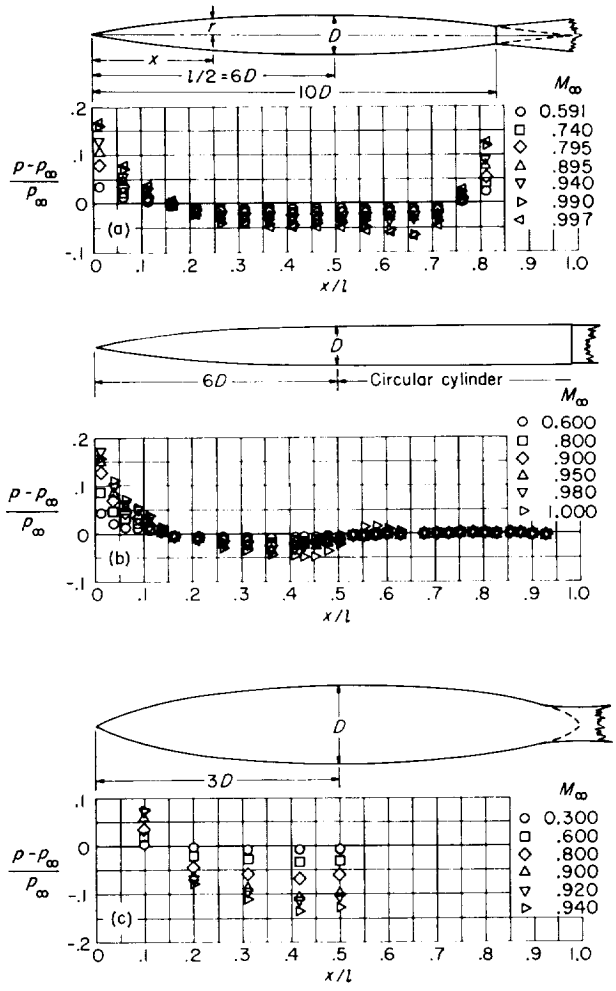

(a) Body of revolution with basic-shape afterbody. $f=12$; $D=3.33$ inches; orifice diameter=0.020 inch. Data are averages of values from references 12 to 14, and from unpublished measurements.

(b) Body of revolution with cylindrical afterbody. $f=12$; D=3.33 inches; orifice diameter=0.030 inch for nose and 0.025 inch for cylinder. Data from reference 15.

(c) Typical transonic body. $f=6$; $D=4$ inches; orifice diameter=0.010 inch. Data from reference 16.

FIGURE 5.—Several bodies of revolution and their experimentally determined surface pressures suitable for use in the aerodynamic compensation for position error ahead of aircraft at subsonic and transonic speeds. $\alpha=0°$; $p_t=1$ atmosphere.

OTHER ERROR CONSIDERATIONS

Combined errors due to sensor position and bow-wave passage.—At supersonic speeds after the aircraft bow wave has moved some distance downstream of the static-pressure orifices in a nose-boom installation, the sensed pressures are unaffected by aircraft disturbances. The free-stream static pressure can then be sensed by means of orifices in cylindrical-tube surfaces of probes designed also to provide induced pressures for compensating position error at subsonic speeds (fig. 6(a)). For such probes the pressures sensed by orifice systems A and B (fig. 6(a)) may be indicated by separate instruments or by a common instrument and appropriate switching between the alternate orifice systems. Automatic switching devices may be actuated by the ratio of static pressure to total pressure or by the differential pressure associated with bow-wave passage.

An arrangement for obtaining, by use of a common system of orifices, approximate free-stream pressures at supersonic speeds and induced pressures suitable for error compensation at subsonic speeds is illustrated in figure 6(b). The aerodynamic basis for this arrangement is associated with fundamental differences between subsonic and supersonic pressure distributions for nose surfaces, as illustrated by body-of-revolution pressure distributions shown in figure 7 (data from refs. 12 to 14 and 18). For the case illustrated in figure 7, it is apparent that approximate free-stream pressures at supersonic speeds and compensation at subsonic speeds may be obtained by a single ring of orifices at $x/l \approx 0.21$ or by several rings of orifices at different axial stations (fig. 6(b)). Other information concerning the use of nose-surface orifices for sensing pressures at supersonic speeds is reported in references 19 and 20.

Combined errors due to sensor position and angle of attack.—At angles of attack other than zero, the sensing of free-stream static pressures by means of aircraft nose-boom pressure installations involves errors associated with changes in the crossflow around the pressure-sensing probe at all speeds and with flow changes in the disturbance field of the aircraft due to changes in angle of attack at subsonic and near-sonic speeds. Figure 8 illustrates the variation of induced circumferential pressure distributions for a probe-type body of revolution at various angles of attack. It is apparent that such variation can cause significant change in the average pressure sensed by interconnected orifices around the circumference of a probe. These variations can be largely avoided by locating pressure-sensing orifices about 37.5° from the bottom (stagnation point of crossflow) of the probe. (See fig. 8 and refs. 20 and

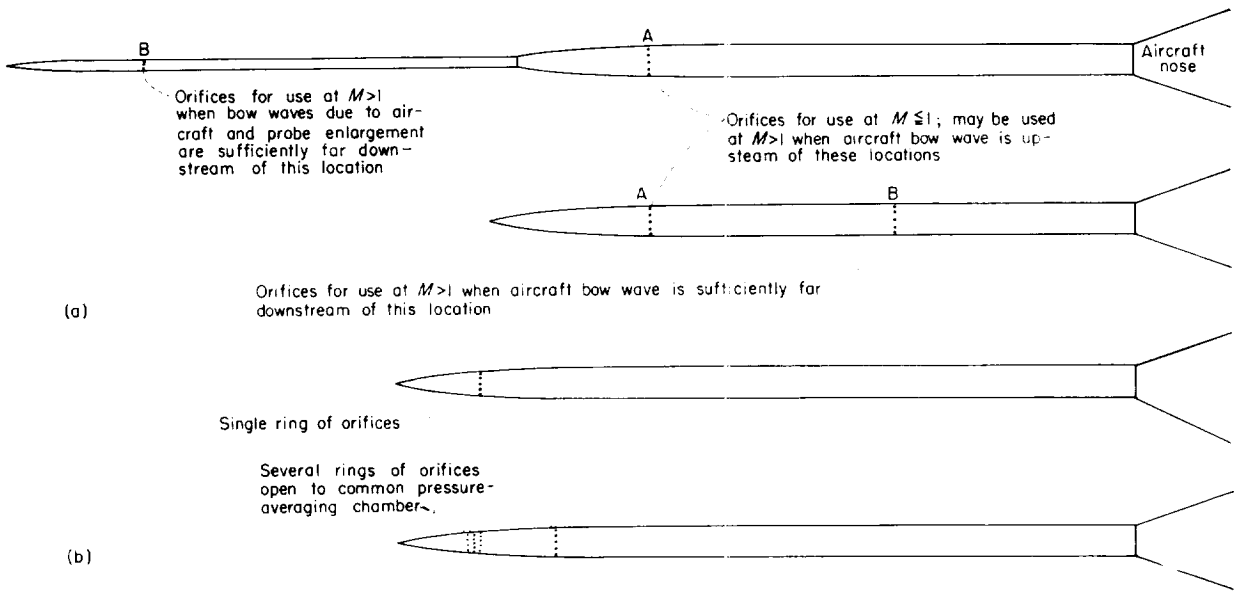

(a) Two systems of orifices, one for use at subsonic and near-sonic speeds and the other for use at supersonic speeds.
(b) Single system of orifices for use at both subsonic and supersonic speeds.

FIGURE 6.—Several arrangements for directly sensing the free-stream static pressure at subsonic and supersonic speeds by means of probe-surface orifices.

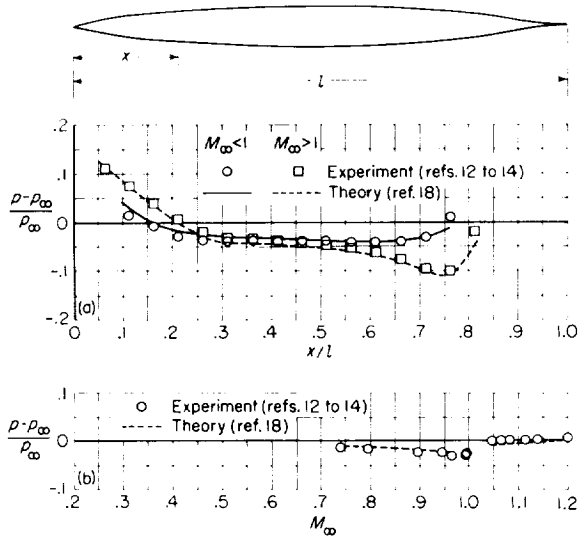

(a) Pressure distributions at subsonic and supersonic speeds.
(b) Variation with Mach number of body-surface pressures at $x/l=0.2125$.

FIGURE 7.—Illustration of pressure-distribution changes with Mach number which permit the selection of body-of-revolution nose orifices for indicating approximate free-stream pressures at supersonic speeds and induced pressures at subsonic speeds. $f=12; \alpha=0°$.

21.) This indicated insensitivity of local probe-surface pressures at $\theta=37.5°$ to angle-of-attack variation was incorporated into the design of probes briefly tested during the present investigation.

Another method for aerodynamically reducing static-pressure error due to inclination of a probe with orifices around the entire circumference involves the simple procedure of designing the probe to sense pressures somewhat larger than free-stream values when the probe is at $\alpha=0°$ in order to extend the attitude range that can be tolerated while the error is kept within acceptable limits. This procedure involves the calculated undercompensation for position error at subsonic and near-sonic speeds and the use of orifice arrangements for providing pressures larger than free stream at supersonic speeds. The use of orifices located at regular close intervals around the entire circumference of the probe then provides for the reduction of error due to probe inclination in any plane. An experimental check of this method was obtained during the present investigation.

APPARATUS

WIND TUNNELS

The tests of the present investigation were conducted in the longitudinally slotted test sections of the Langley 8-foot transonic tunnel and the Langley 8-foot transonic pressure tunnel. A description of the Langley 8-foot transonic

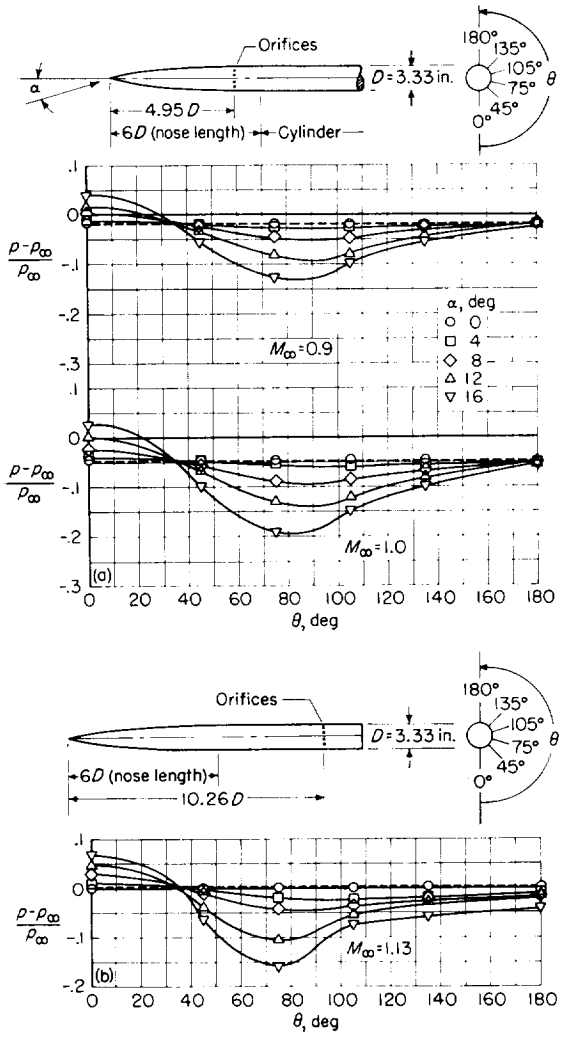

(a) Nose. $M_\infty \leq 1.0$.
(b) Cylindrical afterbody. $M_\infty = 1.13$.

FIGURE 8.—Effect of angle of attack on circumferential pressure distributions at axial stations on nose and on cylindrical portions of a probe-type configuration at transonic speeds. Data from reference 15.

tunnel, including flow and interference characteristics, is given in reference 12. Pertinent details concerning the model support system and the geometry of the test section of the Langley 8-foot transonic pressure tunnel are shown in figure 9. In this facility the open area of the slotted top and bottom walls comprises approximately 5 percent of the total periphery of the test section; the cross-sectional area of the test region is approximately 50 square feet. The humidity is controlled by drying the area in the tunnel to appropriate dewpoints between 0° F and −40° F.

536272—60 —2

MODELS FOR POSITION-ERROR MEASUREMENTS AND PROBE TESTS

Sting-mounted models employed for position-error measurements and for probe tests during the present investigation are shown in figure 10. The models utilized slender, bluff, and intermediate nose shapes to permit experimental studies of position error and probe performance ahead of aerodynamic configurations having different nose shapes. The slender-nose transonic aircraft model included fuselage, wing, and tail surfaces, the principal dimensions and nose ordinates of which are given in figure 10(a). The bluff-nose body of revolution utilized a hemispherical nose as illustrated in figure 10(b). The intermediate-nose body of revolution (fig. 10(c)) utilized a nose shape which simulated that of a subsonic transport airplane. A photograph of the slender-nose model with an aerodynamic-compensation probe extending ahead of the fuselage nose is shown as figure 10(d).

STATIC-PRESSURE TUBES AND PROBES

Tubes for measurement of position error ahead of models.—The static-pressure survey tubes used for measurements of position error ahead of the models shown in figure 10 consisted of 0.375-inch-diameter steel tubing with ogival noses at the upstream ends. The tubes contained 0.031-inch-diameter pressure orifices installed at various axial locations sufficiently far (more than 10 tube diameters) downstream of the tube noses to be essentially uninfluenced by flow gradients due to the noses.

Probes for aerodynamic compensation for position error at subsonic and near-sonic speeds.—Several probes used for aerodynamic compensation for position error ahead of models in this investigation are shown in figure 11(a), and their ordinates are given in table I. Probes 1 and 2 are of the same design and utilize a nose shape similar to the forebody of an extensively tested body of revolution (refs. 12 to 15) for which pressure distributions are given in figures 5(a) and 5(b). A photograph of probe 1 is shown as figure 11(b). Probe 3 utilizes the same nose shape as probes 1 and 2 but the afterbody is indented, as shown in figure 11(a). A photograph of probe 3 is shown as figure 11(c). Probes 4 and 5 are of identical design (fig. 11(a)) and have the nose shape of the "typical transonic body" described in reference 16. All of the probes had the same diameter (0.375

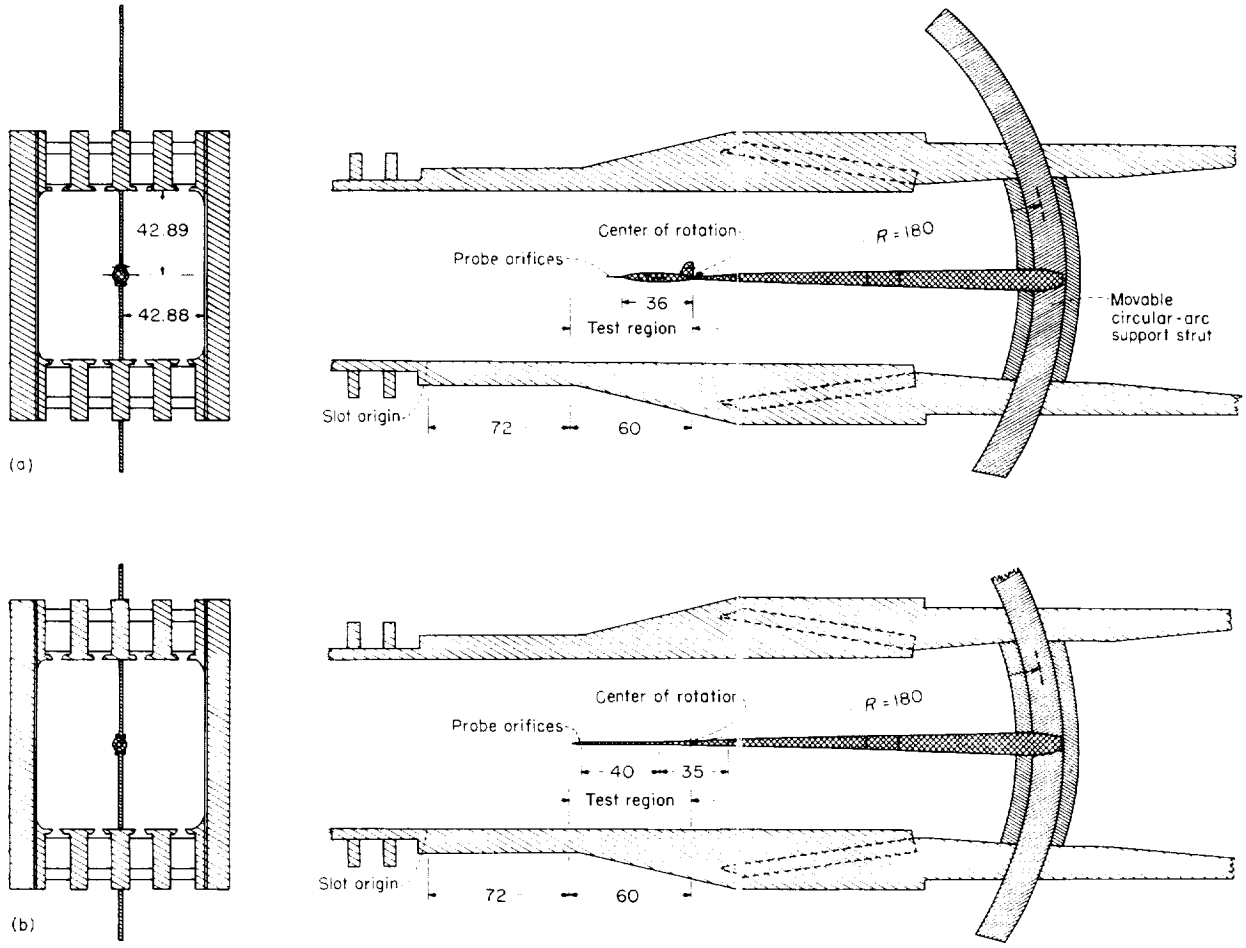

(a) Small-size probe ahead of slender-nose aircraft model.
(b) Large-size probe installed for calibration at transonic speeds.

FIGURE 9.—Sketches of typical arrangements for testing aerodynamic-compensation probes in the Langley 8-foot transonic pressure tunnel. All dimensions are in inches.

in.) and were designed for use with the models shown in figure 10. Probe construction accuracies, as indicated by averages of measurements of radii at four circumferential stations 90° apart, are shown in figure 12. Probe surfaces were maintained smooth and free of appreciable irregularities by use of crocus abrasives applied in the streamwise direction; no measurements of surface roughness were made. Distributed roughness about 0.003 inch high, estimated to be adequate for fixing transition (refs. 22 and 23), was used near the upstream ends of the probe noses (fig. 11(a)) to insure uniform conditions for all tests.

Probes for aerodynamic reduction of combined errors due to position and bow-wave passage.—Probes 1A and 1B, which were used for aerodynamic compensation for position error at subsonic speeds and for sensing free-stream pressures at supersonic speeds, are shown in figure 13; these probes were the same as probe 1 except that additional pressure orifices were installed at selected axial locations. These probes had approximately the same surface conditions and transition-fixing distributed roughness used for probe 1.

Probes for aerodynamic reduction of combined errors due to position and angle of attack.—Probes 1C and 5C, which were used for combining the aerodynamic compensation for position error with a simple method for aerodynamic reduction of static-pressure error due to angle of attack, are shown in figure 14. These probes were the same as probes 1 and 5 except that the pressure orifices used with probes 1 and 5 were filled with solder and at the same axial locations new 0.031-inch-

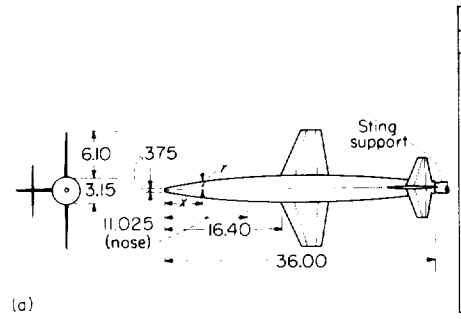

Nose ordinates	
x	r
0	0.188
.5	.292
1.0	.404
1.5	.512
2.0	.616
3.0	.805
4.0	.975
5.0	1.118
6.0	1.235
7.0	1.336
8.0	1.423
9.0	1.494
10.0	1.546
11.025	1.575

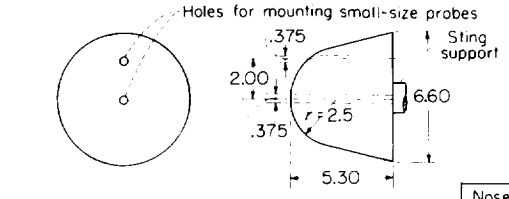

Nose ordinates	
x	r
0	0
.1	.316
.2	.447
.3	.548
.5	.708
1.0	1.000
2.0	1.414
3.0	1.732
4.0	2.000
5.0	2.236
6.0	2.450
7.0	2.646
8.0	2.828
9.0	2.960
10.0	3.000

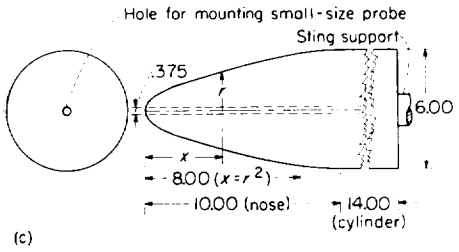

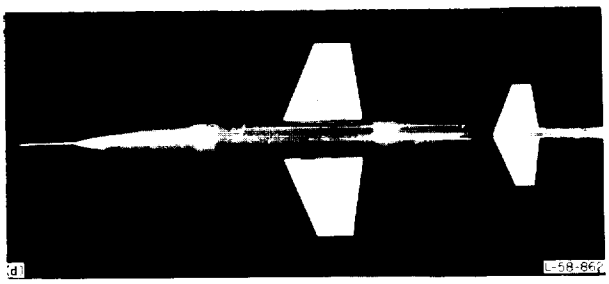

(a) Slender-nose transonic aircraft model.
(b) Bluff-nose body of revolution.
(c) Intermediate-nose body of revolution.
(d) Slender-nose transonic aircraft model with aerodynamic-compensation probe ahead of model nose.

FIGURE 10.—Sting-mounted wind-tunnel models ahead of which aerodynamic-compensation probes were tested and position-error measurements were obtained during the present investigation. Dimensions and ordinates are given in inches.

diameter orifices, opening into a common settling chamber, were circumferentially spaced 75° apart (fig. 14). Probes 1C and 5C had the same surface conditions and transition-fixing roughness used for probes 1 and 5.

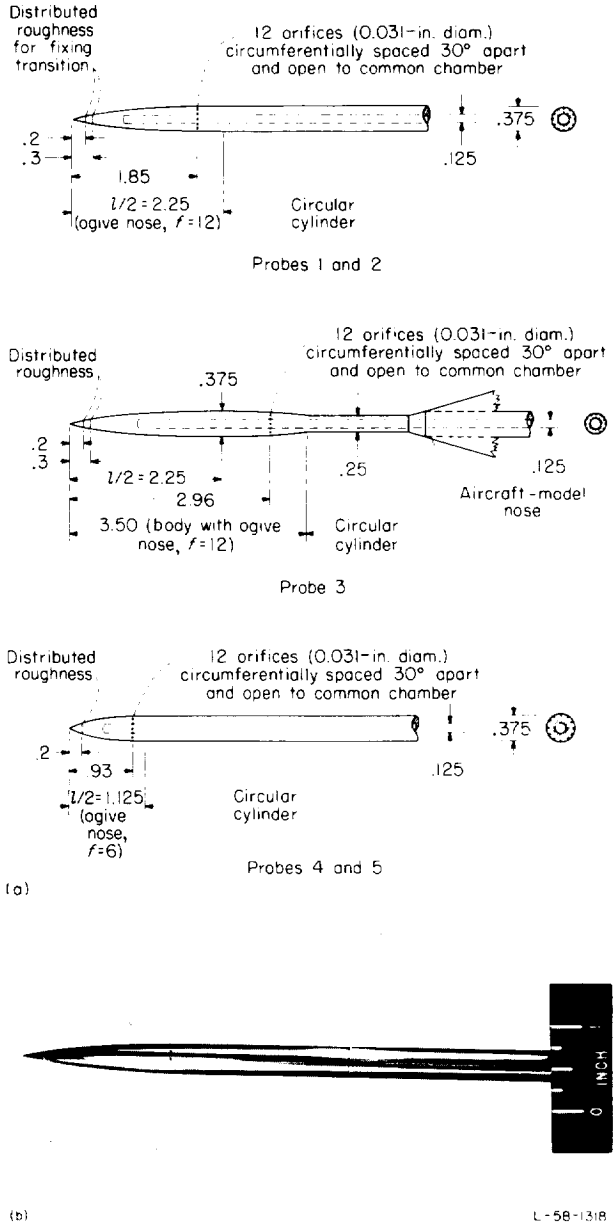

(a) Probe details and dimensions.
(b) Probe 1.

FIGURE 11.—Probes used for experimental verification of induced-pressure method for aerodynamic compensation for static-pressure error due to position. All dimensions are in inches unless otherwise specified.

Large-size probes used for measuring effects due to angle of attack and nose-geometry change.—Probe 6, employed for a brief investigation of the effect of angle of attack on pressures sensed by the probe, is shown in figure 15(a). The downstream portion of the probe was constructed of

TABLE I.—DESIGN ORDINATES FOR NOSES OF PROBES 1 TO 7

Probes 1 and 2

x', in.	y', in.
0	0
.023	.0104
.034	.0134
.056	.0193
.113	.0325
.225	.0542
.338	.0726
.450	.0887
.675	.1166
.900	.1390
1.125	.1559
1.350	.1684
1.575	.1770
2.025	.1865
2.250	.1875

Probe 3

x', in.	y', in.
0	0
.023	.0104
.034	.0134
.056	.0193
.113	.0325
.225	.0542
.338	.0726
.450	.0887
.675	.1166
.900	.1390
1.125	.1559
1.350	.1684
1.575	.1770
2.025	.1865
2.250	.1875
2.475	.1858
2.738	.1810
2.925	.1729
3.150	.1603
3.375	.1408
3.510	.1250

Probes 4 and 5

x', in.	y', in.
0	0
.011	.0104
.017	.0134
.028	.0192
.056	.0325
.112	.0542
.225	.0886
.450	.1391
.675	.1683
.900	.1828
1.125	.1875

Probe 6

x', in.	y', in.
0	0
.060	.0277
.090	.0358
.150	.0513
.300	.0866
.600	.1446
.900	.1935
1.200	.2367
1.800	.3110
2.400	.3708
3.000	.4157
3.600	.4490
4.200	.4719
4.800	.4875
5.400	.4970
6.000	.5000

Probe 7

x', in.	y', in.
0	0.1875
.030	.1935
.330	.2367
.930	.3110
1.530	.3708
2.130	.4157
2.730	.4490
3.330	.4719
3.930	.4875
4.530	.4970
5.130	.5000

1-inch-diameter steel tubing. The nose portion of the probe utilized the same shape as that used for probes 1 and 2; its design ordinates are given in table I and its construction accuracy is indicated in figure 12. Pressure orifices at four axial locations opened into four pressure-averaging chambers

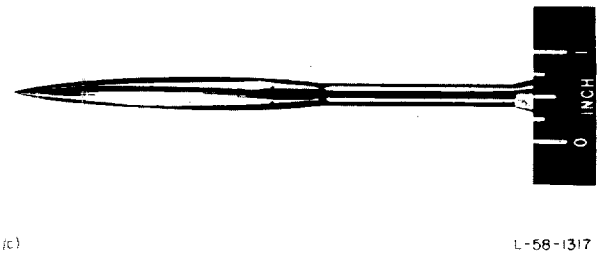

(c) Probe 3.

FIGURE 11. Concluded.

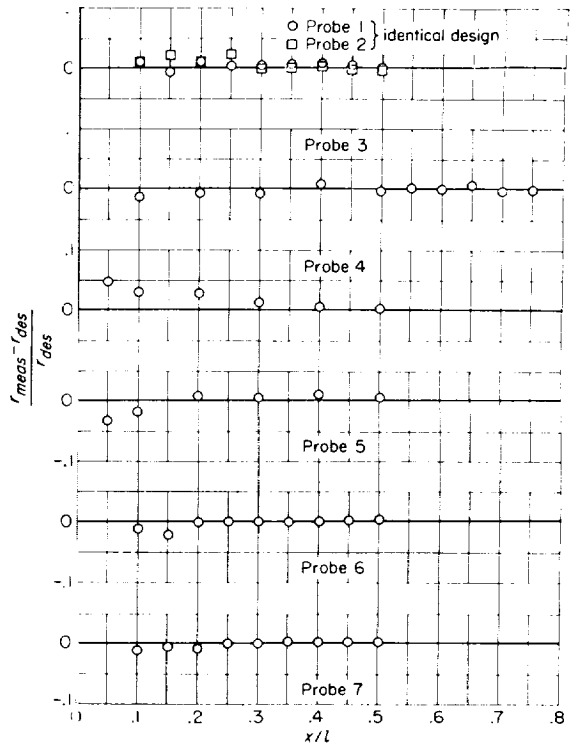

FIGURE 12. Probe construction inaccuracies as indicated by differences between measured and design radii of probes 1 to 7.

from which pressure leads were brought out as shown in figure 15(b).

Probe 7, employed for ascertaining the effect of a nose total-pressure opening on probe-surface induced pressures, is shown in figure 16. The design shape of probe 7 was the same as that of probe 6 except that the upstream tip of probe 7 was cut off for installation of a 0.375-inch-diameter total-pressure opening. The axial location of static-

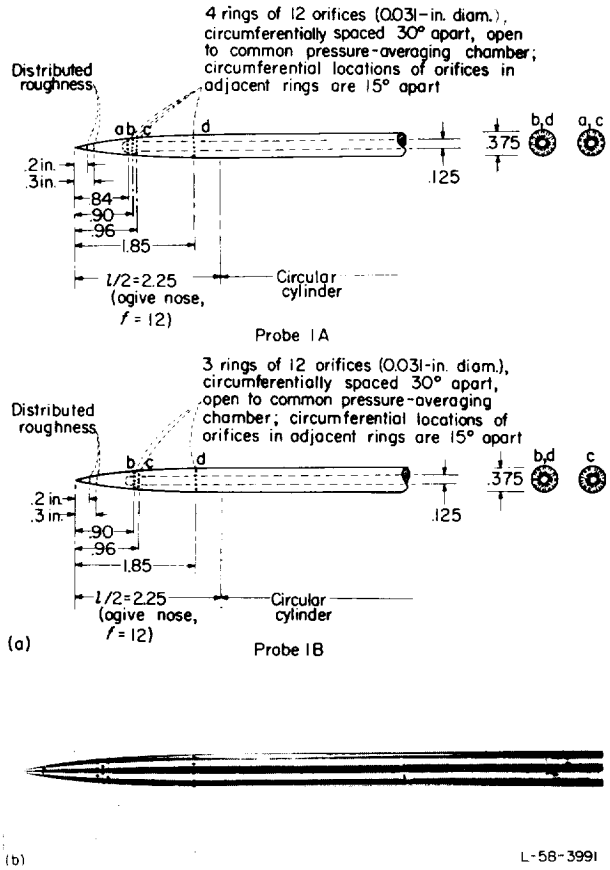

(a) Details and dimensions of probes 1A and 1B.
(b) Probe 1A.

FIGURE 13. Small-size probes for sensing approximate free-stream static pressure at supersonic speeds and aerodynamically compensating for position error at subsonic and near-sonic speeds.

pressure orifices on probe 7, relative to the original nose, was the same as that for orifice location 2 on probe 6.

A cylindrical tube (not shown) of 1-inch diameter was used for measuring the effects of angle of attack on pressures sensed by orifices circumferentially located 30°, 33°, 36°, 37.5°, and 40° from the bottom of the tube. The diameter of the orifices in the tube was 0.031 inch.

TESTS AND DATA

TESTS

Some of the presently reported tests were conducted in the Langley 8-foot transonic pressure

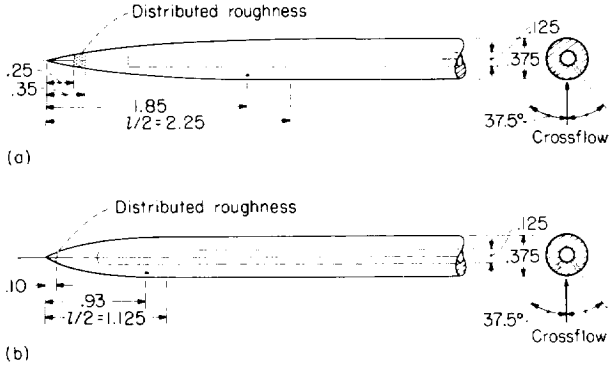

(a) Probe 1C with two orifices (0.031-in. diam.) circumferentially located 37.5° from stagnation point of crossflow.
(b) Probe 5C with two orifices (0.031-in. diam.) circumferentially located 37.5° from stagnation point of crossflow.

FIGURE 14. Probes used for combining aerodynamic compensation for position error with a simple method for aerodynamic reduction of static-pressure error due to angle of attack. All dimensions are in inches unless otherwise specified.

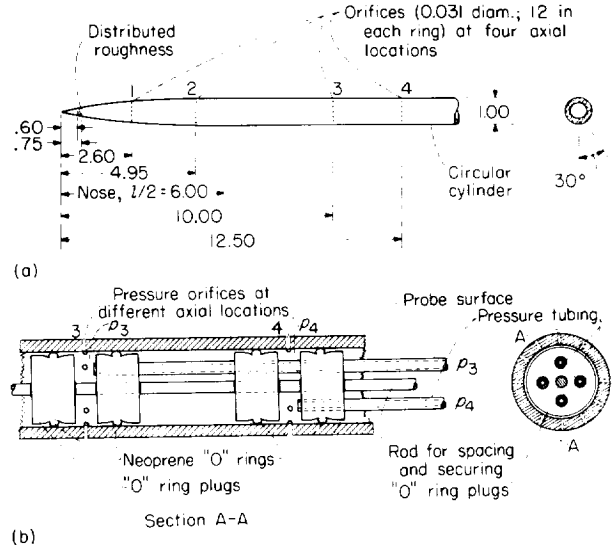

(a) Probe 6.
(b) Illustration of "O" ring technique used for constructing pressure-averaging chambers at different axial locations of orifices for probe 6.

FIGURE 15. Large-size probe and tubes used for measuring the effect of angles of attack on pressures sensed by orifices at four axial locations. All dimensions are in inches unless otherwise specified.

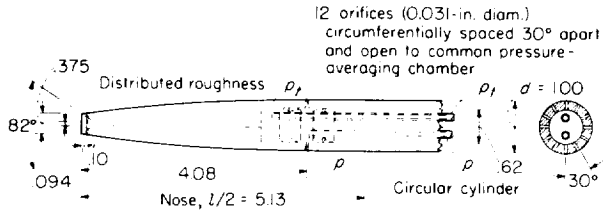

FIGURE 16.—Large-size probe 7 used for determining the effect of a total-pressure opening on static pressures at orifices located 4.08 diameters from the nose. All dimensions are in inches unless otherwise indicated.

tunnel and others were performed in the Langley 8-foot transonic tunnel. The testing characteristics of these tunnels were approximately the same and no appreciable differences in test results appeared likely. The principal measurements obtained during the presently reported tests included average static pressures in the tunnels and average pressures sensed by the investigated static-pressure probes. These measurements were generally obtained by visually reading or by photographically recording the heights of tetrabromoethane in multiple-tube manometers connected to the pressure orifices or chambers concerned. Tunnel stagnation pressures were accurately measured by means of an absolute-pressure manometer. Schlieren pictures were obtained when possible to supplement the pressure measurements.

The tests utilized flow calibrations similar to those described in reference 12 which used as a basis of reference the ratio of the stream total pressure to the pressure in the tank surrounding the slotted test section. The calibrations were for the particular regions at which the pressure-sensing orifices on the probes were located for testing.

The angles of attack of the models and probes were varied by means of the movable circular-arc support struts. The centers of rotation of the circular-arc struts were located somewhat downstream of the probe pressure orifices (fig. 9), so that there were small displacements of the pressure-sensing orifices from the tunnel center lines at large angles of attack.

The relative humidity in the Langley 8-foot transonic tunnel was generally controlled by heating to avoid saturation conditions in the test section for both flow calibration and probe tests. In the Langley 8-foot transonic pressure tunnel drying was employed, as previously noted, to minimize humidity effects.

The effectiveness of distributed roughness employed for fixing transition during the present tests was not experimentally checked.

The test conditions included Mach numbers from about 0.4 to 1.2, angles of attack from 0° to 8°, and Reynolds numbers from 2.3×10^6 to 4.2×10^6 per foot. A comparison of wind-tunnel and flight Reynolds numbers is shown in figure 17.

DATA REDUCTION

Free-stream Mach numbers were obtained from appropriate test-region flow calibrations for ratios of measured stagnation pressures to measured pressures in the tank surrounding the slotted test

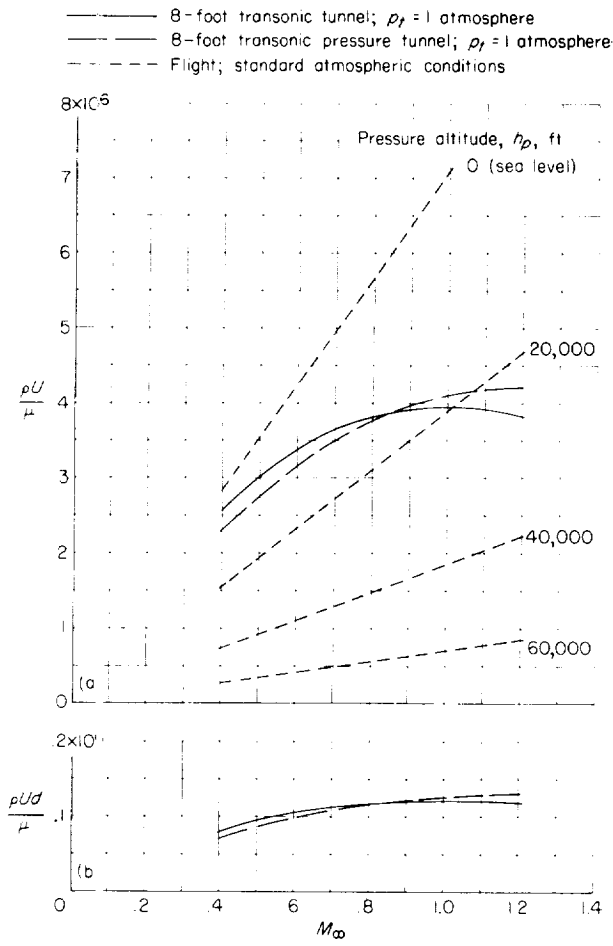

(a) Reynolds number per foot.

(b) Reynolds number based on linear dimension equal to probe diameter of 0.031 foot and wind-tunnel test conditions.

FIGURE 17.—Reynolds numbers for transonic-wind-tunnel tests at atmospheric stagnation pressure and for flight at standard atmospheric conditions.

section. Free-stream static pressures were obtained from the free-stream Mach numbers and the stagnation pressure by use of isentropic-flow tables.

The probe-test results were generally presented in terms of the static-pressure-error parameter $\frac{p-p_\infty}{p_\infty}$, which could be readily interpreted in terms of altitude error (as previously illustrated in fig. 2) or in terms of errors in other air-data parameters. The position-error measurements were expressed in terms of a parameter $(l/D)^2 \frac{p-p_\infty}{p_\infty}$, which was a modification of the parameters used in references 1 and 9. Reference 24 presents simple equations for relating the various air-data parameters.

No corrections for boundary interference have been applied to data from the present investigation. Interference effects are believed to be negligible at subsonic speeds but appreciable at low supersonic speeds where disturbances from the test-section boundary may influence the flows at and upstream of the regions occupied by the pressure-sensing orifices on the probes (refs. 12 and 25). The supersonic speed ranges within which boundary-reflected disturbances may influence the probe pressures are indicated in the data plots.

PRECISION

At subsonic and sonic speeds the maximum random error in measuring the difference between the local or probe-indicated static pressure p and the tunnel reference pressure p_{TC} by use of a liquid manometer was estimated to be less than 1.5 pounds per square foot, and the assumption of an equal maximum error associated with the accuracy and repeatability of tunnel flow calibrations yields a possible maximum error of approximately 3 pounds per square foot. This combined error is equivalent to values of ΔM less than 0.003 and to values of $\frac{p-p_\infty}{p_\infty}$ ranging from 0.0016 at $M_\infty=0.4$ to 0.0027 at $M_\infty=1.0$.

At supersonic speeds the maximum random error in determining Δp (that is, $p-p_\infty$) largely depends upon test-region flow nonuniformities which vary with Mach number. At some supersonic speeds outside the region of possible influence of boundary-reflected disturbances on probe data, the maximum absolute error may be about the same as that at subsonic speeds, whereas at others it may be sufficient to produce values of ΔM greater than 0.004 and values of $\frac{p-p_\infty}{p_\infty}$ near 0.005.

The maximum error in determining the attitude of a model or probe with respect to the average direction of the airstream was estimated to be about 0.2°.

RESULTS AND DISCUSSION

POSITION-ERROR MEASUREMENTS

The results of the present position-error-measurement tests, which were conducted to supplement existing position-error information in references 1 and 9, are given in figure 4. These data are presented in the form of curves showing the variation of the error parameter $(l/D)^2 \frac{p-p_\infty}{p_\infty}$ with distance x/l at Mach numbers from 0.40 to 1.02. The present test data, which include position-error measurements ahead of the three bodies of figure 10, are in relatively close agreement with one another and with data from references 1 and 9. This data correlation affords evidence concerning the satisfactory agreement of flight and wind-tunnel data and the general adequacy of the employed error parameter for relating position-error data for different aerodynamic configurations. The faired curves shown in figure 4 appear generally suitable for estimating the position error ahead of arbitrary configurations, although these curves may be inadequate for accurately predicting the error at axial locations very near configurations having bluff noses or abrupt shoulders near the nose. The data of figure 4 also indicate that the magnitude of the position error ahead of a slender-nose configuration is somewhat smaller at $\alpha=8°$ than it is at $\alpha=0°$, as expected.

AERODYNAMIC COMPENSATON FOR POSITION ERROR

Experimental verification of error-compensation method.—The results of wind-tunnel tests conducted to investigate the error-compensation performance of probes 1, 3, and 4 (fig. 11(a)) at three selected locations ahead of the slender-nose aircraft model (fig. 10(a)) are shown in figure 18. These results were obtained from single-attempt tests based on estimates (using data from figs. 4 and 5) designed to yield the smallest maximum

static-pressure error for Mach numbers up to about 1.02. The data of figure 18(a) show the adequacy of probe 1 for aerodynamically compensating the position error at a location 0.87 fuselage diameter ahead of the model nose for Mach numbers from 0.4 to slightly above 1.0. The resultant static-pressure error with compensation is shown to be less than 0.5 percent up to a Mach number slightly greater than 1.0. The data of figure 18(b) illustrate the suitability of probe 3 for aerodynamically compensating the position error at a location 0.79 fuselage diameter ahead of the model nose for Mach numbers up to 1.0. The resultant static-pressure error with compensation is less than 0.5 percent. Similar data for probe 4 are shown in figure 18(c). In this case the very large position error at a location 0.27 fuselage diameter ahead of the model nose is compensated within 0.5 percent of the static pressure at Mach numbers up to nearly 1.0. In each of the three instances shown in figure 18, the indicated differences between estimated and measured errors with compensation are sufficiently small to be within maximum possible inaccuracies associated with the techniques employed for error estimates and measurements.

The test results shown in figure 18 constitute an experimental verification of the method used herein

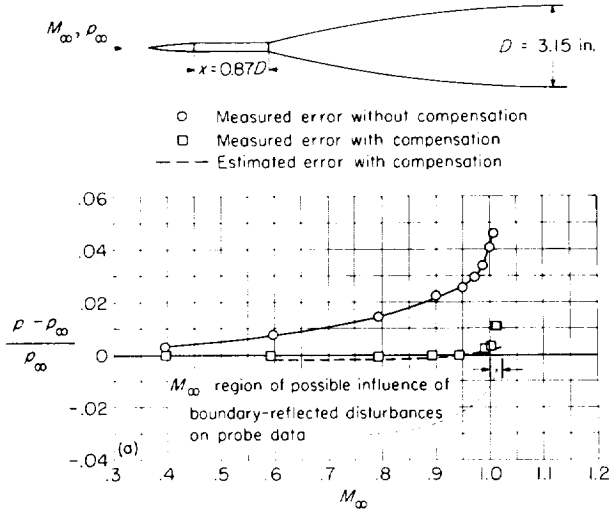

(a) Probe 1 with orifices located 0.87 fuselage diameter ahead of model.

FIGURE 18. Experimental verification of method employed for aerodynamic compensation for position error as provided by tests of small-size probes ahead of slender-nose aircraft model in the Langley 8-foot transonic tunnels. $\alpha = 0°$; $p_t = 1$ atmosphere.

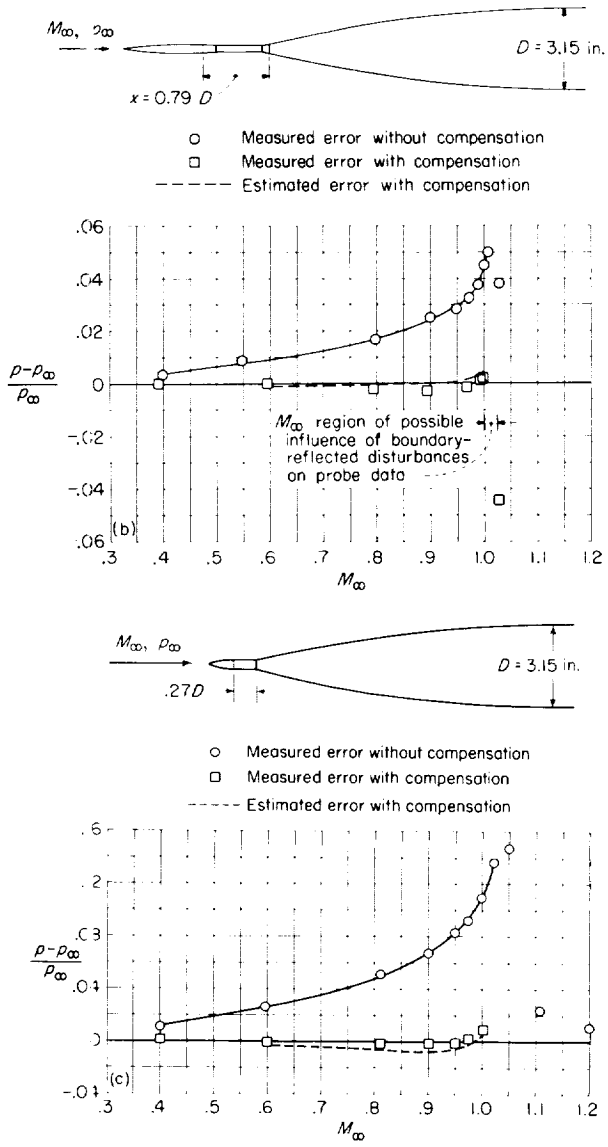

(b) Probe 3 with orifices located 0.79 fuselage diameter ahead of model.

(c) Probe 4 with orifices located 0.27 fuselage diameter ahead of model.

FIGURE 18.—Concluded.

for aerodynamic compensation for position error at subsonic and near-sonic speeds. The results also indicate that position errors at various locations from 0.27 to 0.87 fuselage diameter ahead of a slender-nose configuration can be aerodynamically compensated by use of appropriate probe shapes to yield free-stream static pressure with resultant error of less than 0.5 percent, which is equivalent to an altitude error of about 100 feet,

throughout the range of Mach numbers from 0.4 to about 1.0.

Repeatability of error compensation.—Probe 2 of the same design as probe 1 was tested to check repeatability of the results. Figure 19 shows the excellent agreement between the performances of probes 1 and 2 which, incidentally, were constructed in different machine shops and tested in different wind tunnels. Indicated differences in the data for the two probes are within the estimated precision of measurements.

Sensitivity of aerodynamic compensation to axial location of probe.—The sensitivity of aerodynamic-compensation performance of a probe to axial location of the probe ahead of the aircraft model or configuration may be illustrated by examining the data of probe 1 obtained at several locations ahead of the slender-nose model (fig. 20). These data indicate that the measured static-pressure error with compensation changes in the manner to be expected when the probe location is changed. For example, a comparison of data for locations 0.87 and 0.95 fuselage diameter ahead of the model indicate that this 9-percent change in the probe location yields appreciable but acceptable pressure-error differences in the expected direction at near-sonic and high subsonic speeds.

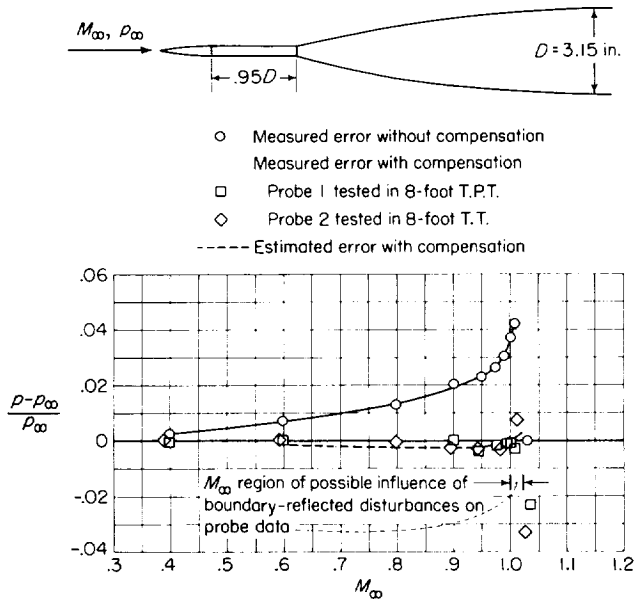

FIGURE 19.—Illustration of repeatability of position-error compensation as indicated by tests of two probes of the same design (probes 1 and 2) at an axial location 0.95 fuselage diameter ahead of the slender-nose model. $\alpha=0°$; $p_t=1$ atmosphere.

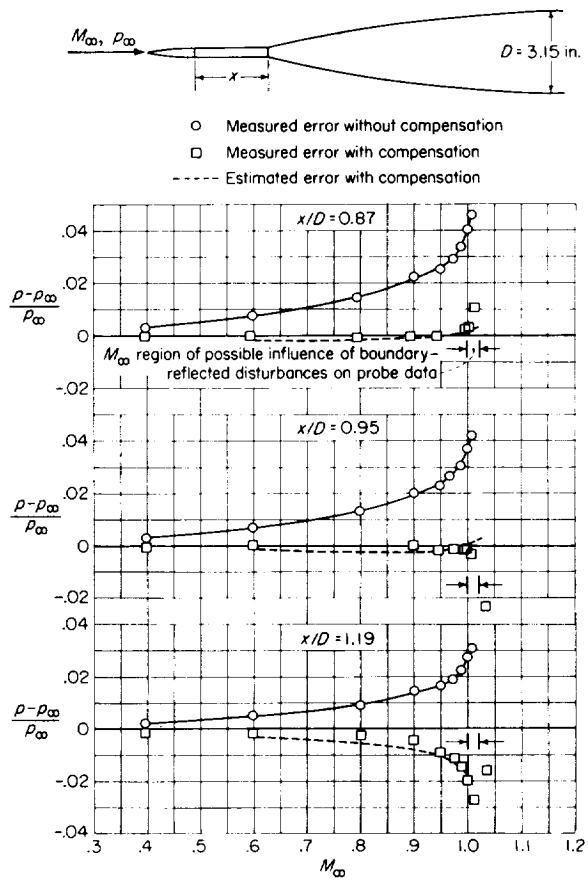

FIGURE 20. Illustration of sensitivity of aerodynamic-compensation performance of probe to axial location of probe as indicated by tests of probe 1 at several locations ahead of the slender-nose model. $\alpha=0°$; $p_t=1$ atmosphere.

For a location 1.19 fuselage diameters ahead of the model large pressure-sensing errors occur in the direction of overcompensation.

Influence of probe-geometry modifications.—Gradual enlargement of the downstream portion of a nose-boom pressure installation is sometimes desirable for structural considerations and for locating pressure-transducing equipment near the pressure-sensing orifices. Such an enlargement of the downstream portion of probe 1 is shown (fig. 21) to have negligibly small influence on the error-compensation performance of the probe.

A nose-shape modification due to the installation of a total-pressure opening at the upstream end of aerodynamic-compensation probe 7 (fig. 16) was shown to produce small pressure-sensing changes (fig. 22(a)) notwithstanding severe flow

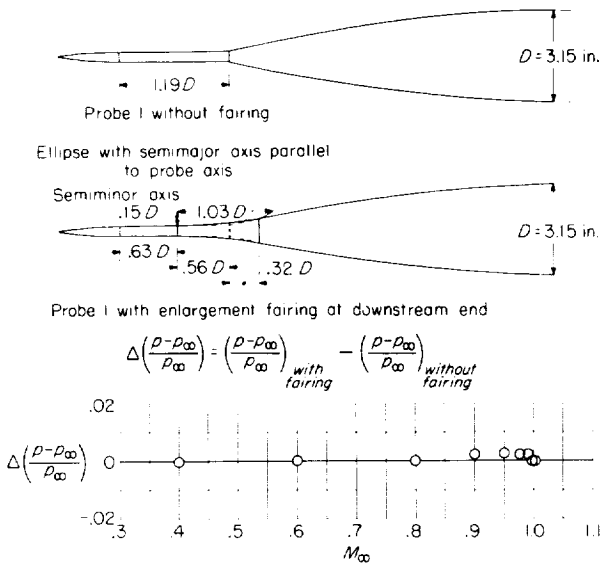

FIGURE 21. Illustration of negligibly small influence of gradually enlarging the downstream portion of the nose boom on the performance of an aerodynamic-compensation probe ahead of the slender-nose aircraft configuration. $\alpha = 0°$; $p_t = 1$ atmosphere.

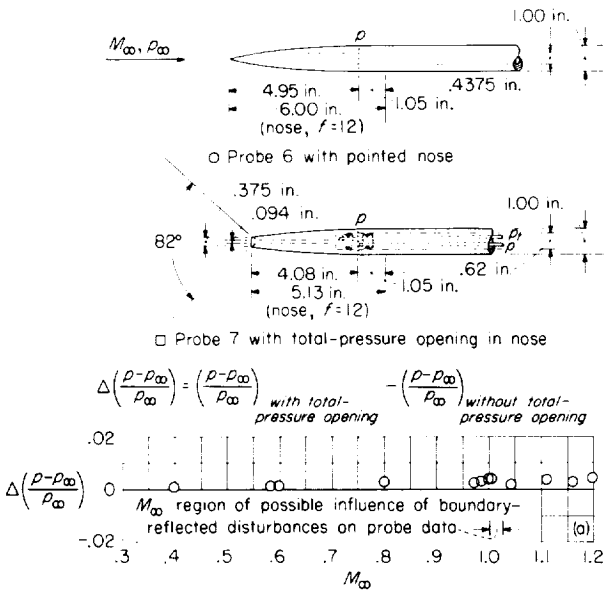

(a) Differences between static pressures sensed by probe 7 and orifices at location 2 on probe 6.

FIGURE 22. Illustration of the influence of a total-pressure opening on the performance of an aerodynamic-compensation probe. $\alpha = 0°$; $p_t = 1$ atmosphere.

disturbances ahead of the static-pressure orifices (fig. 22(b)).

Error-compensation difficulties arising from model bluffness and associated pressure gradient. The error-reduction performances of probes 4 and 5C tested ahead of the bluff-nose body (fig. 10(b)) are shown in figure 23(a). At a location on the body center line about 0.93 body diameter ahead of the body nose, the estimated reduction in error by means of compensation was not fully realized by use of probe 4 (fig. 23(a)). The reason for this performance appeared to be associated with the positive pressure gradient which was sufficiently severe to promote flow separation (fig. 23(b)) and to prevent the attainment of desired probe-induced pressures.

In an attempt to avoid some of the difficulty experienced in aerodynamically compensating for position error for the bluff-nose body, probe 5C was tested off the body center line as shown in figure 23(a). For this test the probe was properly oriented to avoid likely effects of upflow. The test results, presented in figure 23(a), indicated that the aerodynamic compensation of probe 5C at a location 0.93 body diameter ahead of the bluff-body nose and off the body axis was essentially the same as that of probe 4 tested on the body center line. With this same off-center arrangement a 49-percent extension of the pressure-sensor location from 0.93 to 1.39 body diameters ahead of the body approximately equivalent to the length of the separated-flow region shown in figure 23(b)) was necessary in order to compensate aerodynamically for the static-pressure error with an accuracy of 0.5 percent at Mach numbers up to nearly 1.0. Figure 23(a) also includes data which show that, for a Mach number of about 0.9, the aerodynamic-compensation performance of probe 5C was essentially the same for angles of attack of 0° and 4°. A slightly different indicated probe performance for $\alpha = -4°$ was associated with the improper orientation of probe orifices for this attitude.

The results of testing probe 5 with pressure orifices located 0.75 body diameter ahead of the intermediate-nose body of figure 10(c), such as might be employed for a subsonic transport configuration, are shown in figure 24. These test results indicate that probe 5 adequately compensated the position error with a resultant static-pressure error of less than 0.5 percent at Mach numbers from 0.4 to 0.92 for angles of attack of 0° and 6°. The experimentally determined suitable location for probe 5 was about 36 percent farther upstream from the body nose than that estimated. This difference in estimated and experimentally determined probe locations for accurate performance was again approximately equal to the

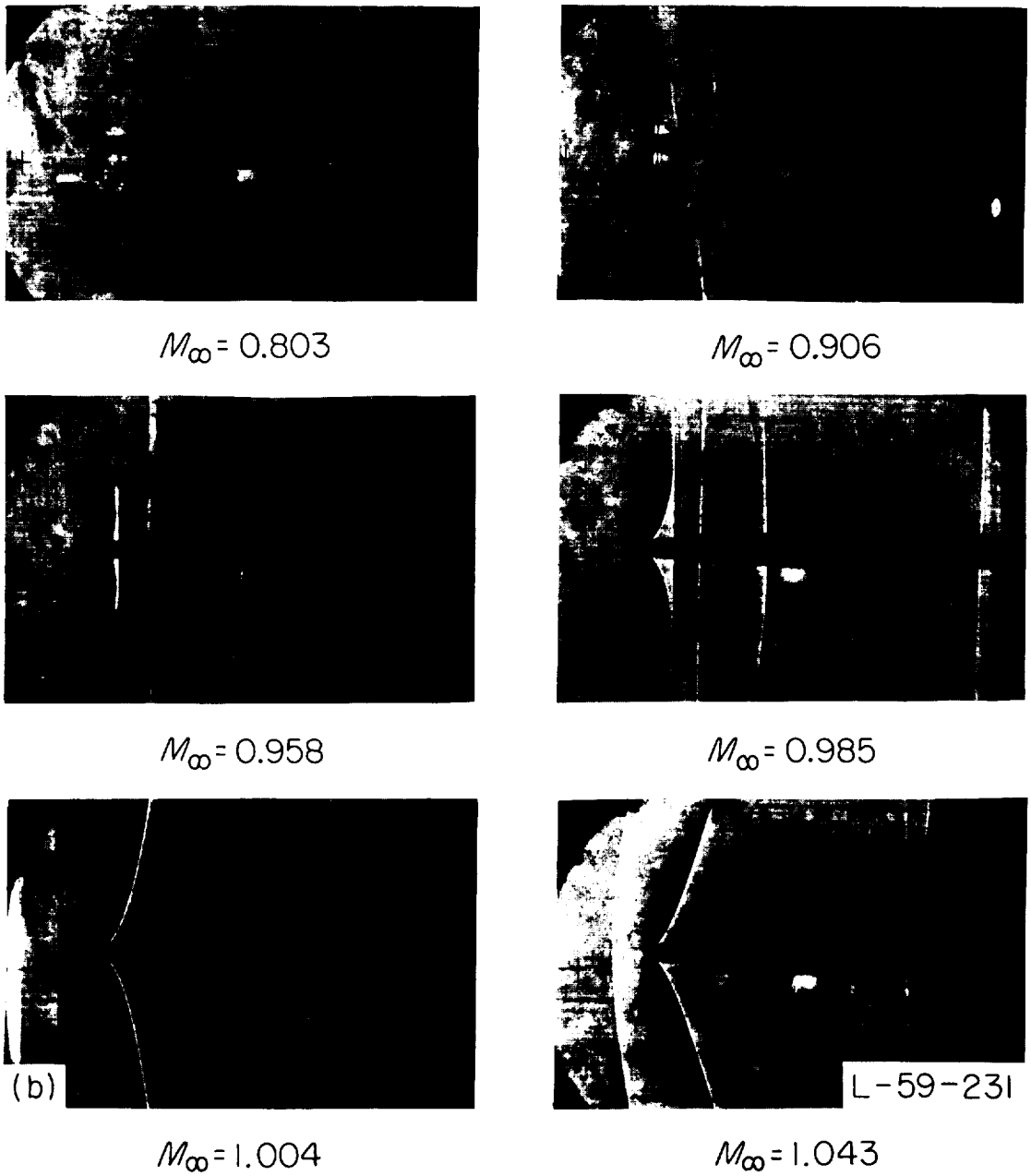

(b) Schlieren pictures of flow field about probe 7.

FIGURE 22.—Concluded.

length of the region of separated flow observed ahead of the nose.

The occurrence of separated flow ahead of models, previously noted for the bluff-nose and intermediate-nose bodies, was not observed for the slender-nose configuration. For the slender-nose configuration, estimated and measured probe performances were in close agreement (fig. 18).

A correlation of observed differences between estimated and measured performances of aerodynamic-compensation probes ahead of slender-nose, intermediate-nose, and bluff-nose bodies indicated that probe-sensed pressures were larger than estimated pressures by amounts which consistently varied with model bluffness and associated severity of flow gradient. Whereas such differences might be negligibly small for applications involving slender-nose aircraft or model

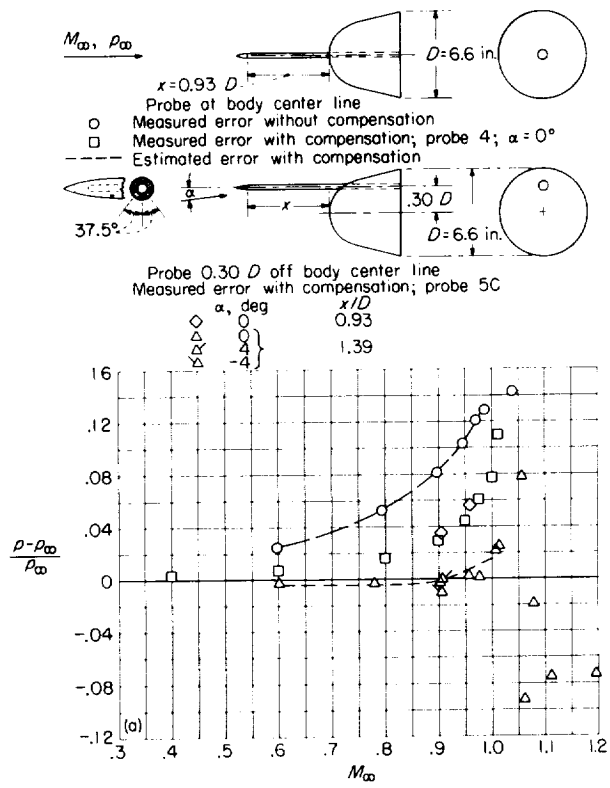

(a) Position error without and with compensation.

FIGURE 23. Experimental check of position error afforded by probes ahead of bluff-nose body of revolution. p_t, 1 atmosphere.

configurations, they could be large for cases involving bluff-nose and intermediate-nose configurations for which the extent of the separated flow region must be considered.

AERODYNAMIC REDUCTION OF COMBINED ERRORS DUE TO POSITION AND BOW-WAVE PASSAGE

This investigated method for directly sensing free-stream pressure at low supersonic speeds and aerodynamically compensating for position error at subsonic speeds involved the use of probe designs 1A and 1B (fig. 13). Tests of these probes at a location 1.19 body diameters ahead of the slender-nose body of figure 10(a) yielded the results shown in figure 25. Pressures slightly larger than free-stream values were indicated by probe 1A at low supersonic speeds. Pressures larger than free stream indicated by probe 1A were reduced to values somewhat lower than free-stream pressures by closing the upstream ring of orifices as shown by the data applying to probe 1B in figure 25. These results demonstrated the feasibility of designing a single system of probe orifices for accurately sensing free-stream static pressure at low supersonic speeds and aerodynamically compensating for position error at subsonic and near-sonic speeds. With this orifice system the static-pressure error is again less than 0.5 percent at subsonic speeds and at supersonic speeds up to $M \approx 1.15$. Slightly larger error occurs at $M > 1.15$. Further reduction of the error at supersonic speeds appeared possible by additional refinement of design, but this was considered unnecessary for the present tests of small-size probes.

Probes such as 1A and 1B (designed for use at both subsonic and low supersonic speeds) generally yield smaller induced pressures, and thus require longer nose booms, than do probes such as 1 to 5 (designed for use only at subsonic and near-sonic speeds). Also, at supersonic speeds the near-free-stream pressures indicated by probes similar to 1A and 1B generally become more positive with increase in Mach number. Improvements in probe performances at supersonic speeds may be afforded by design refinements.

AERODYNAMIC REDUCTION OF COMBINED ERRORS DUE TO POSITION AND ATTITUDE

Effect of probe inclination on sensed pressures.—The effect of probe inclination on average pressures sensed by an isolated probe with orifices distributed around its entire circumference is illustrated by experimental data in figure 26. These data were obtained from calibration tests of probe 6 (fig. 15(a)) supported in the wind-tunnel test section as shown in figure 9(b). The data of figure 26 showed that inclination of the probe with respect to the airstream direction produced probe-indicated pressures which were generally lower than pressures for zero inclination. The magnitude of this effect, expressed in terms of error in sensing free-stream static pressure, increased with increase of Mach number and probe inclination. This information indicated that fairly large probe inclinations may be tolerated at low subsonic speeds, whereas only small deviations from zero inclination are permissible at near-sonic speeds if the static-pressure error is to be kept within 0.5 percent for a probe with orifices distributed around its entire circumference.

The effect of a probe angle of attack of 12° on pressures sensed by orifices circumferentially located 30°, 33°, 36°, 37.5°, and 40° from the

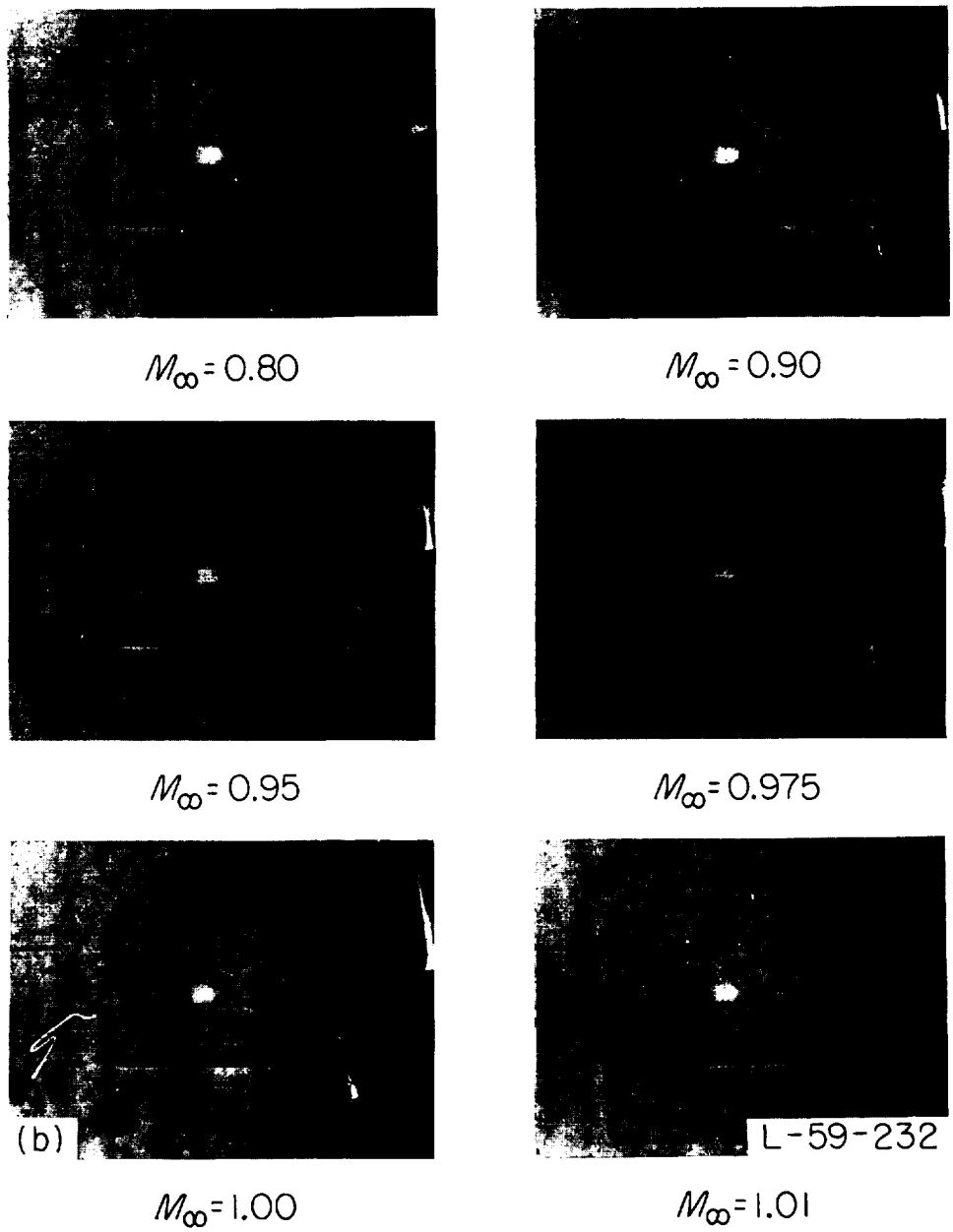

(b) Schlieren pictures showing separated flow in boundary layer of probe 4 ahead of, and on axial center line of, bluff-nose body of revolution. $\alpha = 0°$.

FIGURE 23.—Concluded.

bottom of a cylindrical tube is illustrated by experimental data in figure 27. The data of figure 27 also include pressures sensed by orifices circumferentially spaced 30° apart around probe 6 at location 4 (figs. 15(a) and 26). The results indicated that orifice locations about 37.5° from the stagnation point of the crossflow around a cylindrical tube were satisfactory for sensing approximate free-stream static pressures at Mach numbers from 0.4 to 1.2 for angles of attack as large as 12°. The adequacy of the 37.5° orifice location for providing free-stream pressures at higher supersonic speeds is indicated by data in references 20 and 21.

Effect of body angle of attack on position error.—No detailed measurement of position-error variation with body angle of attack was included

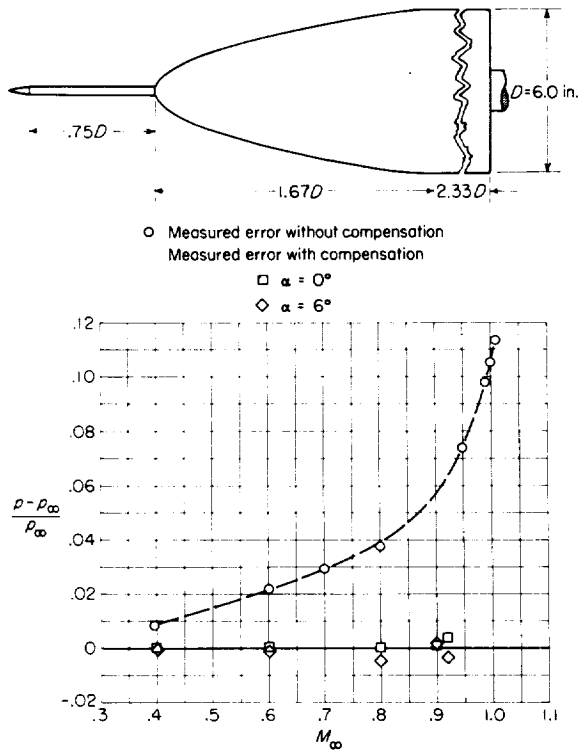

FIGURE 24.—Experimental check of position-error compensation afforded by probe 5 installed ahead of intermediate-nose body of revolution. Pressure-sensing orifices located 0.75 diameter ahead of body nose. $p_t = 1$ atmosphere.

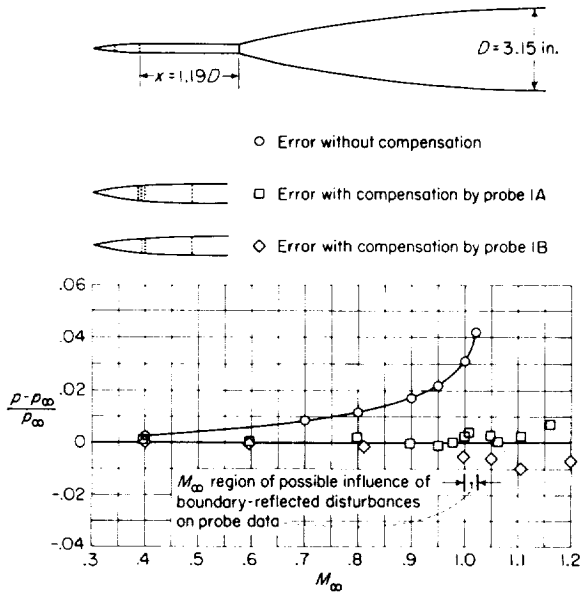

FIGURE 25.—Experimental performance of probes 1A and 1B tested ahead of the slender-nose model. $\alpha = 0°$; $p_t = 1$ atmosphere.

in the present investigation but some limited information was obtained as a byproduct of other related measurements. These included static-pressure measurements showing the magnitude of position error at a location 0.87 body diameter ahead of the slender-nose model at angles of attack of 0° and 8° (fig. 28). The measurements indicated that the position error at $\alpha = 8°$ was less than that at $\alpha = 0°$, which was in the proper direction. Approximate compensation for position-error variation with body angle of attack may be combined with the compensation for error due to probe inclination.

Aerodynamic reduction of static-pressure errors due to position and angle of attack.—Probe 1C (fig. 14) having the orifice location at 37.5° for compensation for both position and angle-of-attack error is seen from figure 28 to be effective in keeping the resultant static-pressure errors, essentially the same for angles of attack of 0° and 8°, to within 0.5 percent at Mach numbers up to about 1.0. Although this excellent error-reduction performance is limited to inclinations in the angle-of-attack plane for the case of a fixed probe (such as the one tested), it may be realized for inclinations in other planes by designing the pressure-sensing portion of the probe to rotate about the probe axis and automatically locate the orifices 37.5° from the stagnation point of the crossflow.

Another simple method of combining compensation for angle-of-attack error with position-error compensation yielded the results shown in figure 24. The investigated technique involved the calculated undercompensation of position error at $\alpha = 0°$ in order to minimize errors due to angle of attack for the case of a probe with orifices located around its entire circumference. The measurements of figure 24 were obtained by use of probe 5 (fig. 11) at a location 0.75 body diameter ahead of the intermediate-nose body at angles of attack of 0° and 6°. The resultant static-pressure errors with compensation were slightly positive at $\alpha = 0°$ whereas they were slightly negative at $\alpha = 6°$, but in no instance did the error exceed 0.5 percent at Mach numbers up to 0.92 (fig. 24). Similar performance is to be expected for inclination in planes other than angle of attack because of the close and symmetrical distribution of orifices around the entire circumference of the probe. Because of its simplicity and its independence of the plane of inclination, this technique appears particularly

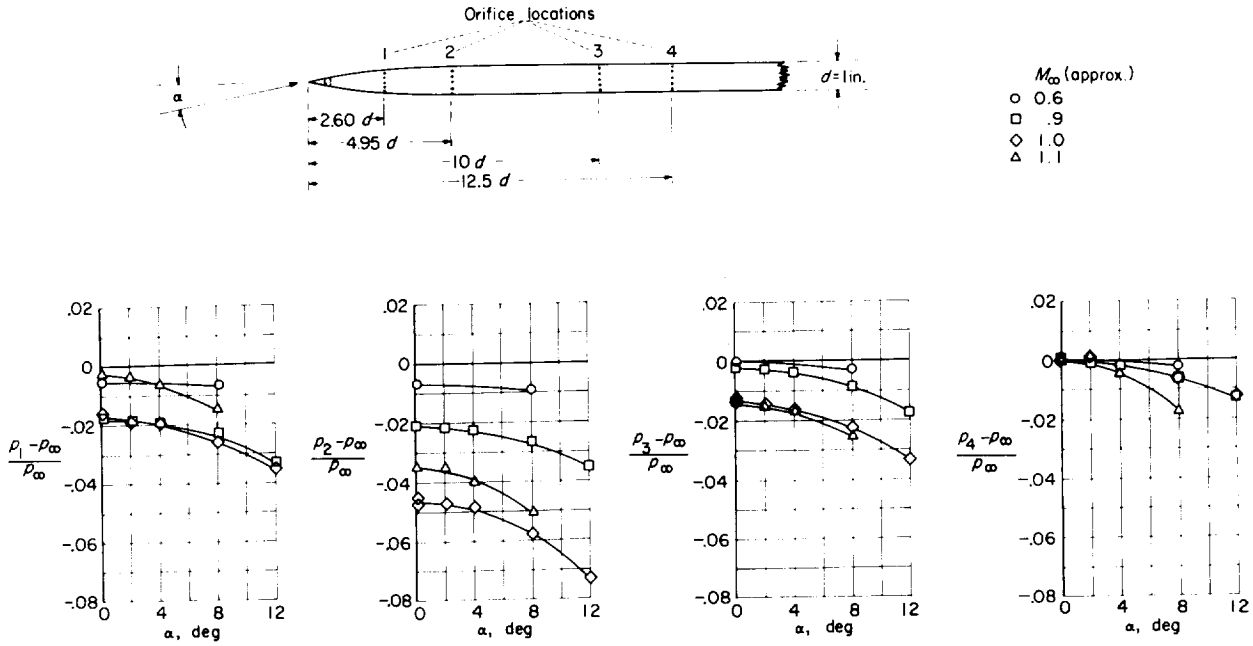

FIGURE 26.—Effect of angle of attack on pressures sensed by orifices at four axial locations for probe 6. Orifice diameter=0.031 inch; p_t=1 atmosphere.

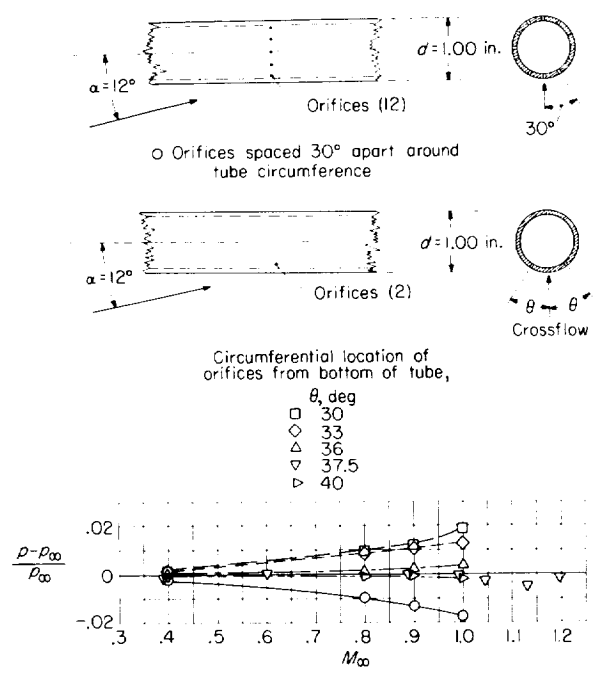

FIGURE 27.—Effect of Mach number on static pressures sensed by orifices at various circumferential locations around cylindrical portions of probes at $\alpha=12°$. p_t=1 atmosphere; orifice diameter=0.031 inch.

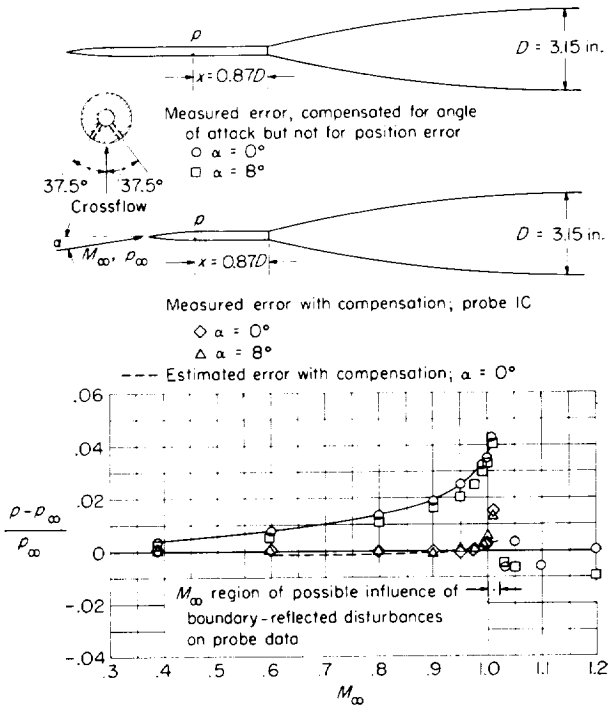

FIGURE 28.—Experimental performance check of probe 1C which utilizes induced pressures for aerodynamic compensation for position error and orifices circumferentially located 37.5° from the stagnation point of the crossflow for reducing errors due to angle of attack. p_t=1 atmosphere.

suitable for use in connection with pressure-sensing systems of aerodynamic missiles, provided the flow angles remain small or moderate.

CONCLUSIONS

Several methods for aerodynamic reduction of errors in sensing static pressures from aircraft at subsonic, near-sonic, and low supersonic speeds were investigated by tests in transonic wind tunnels. The results warranted the following conclusions, which are applicable for the employed ranges of test conditions:

1. Position-error measurements ahead of several aerodynamic configurations tested in wind tunnels were in close agreement with related flight data, and the combined information provided a suitable means for estimating position error ahead of aircraft configurations.

2. A method for aerodynamic compensation for position error by means of probe-surface induced pressures was experimentally verified. The method permitted the direct indication of free-stream static pressure with an error of less than 0.5 percent at subsonic and near-sonic speeds.

3. The direct indication of free-stream static pressures provided by aerodynamic compensation for position error at subsonic and near-sonic speeds was extended to supersonic speeds by means of an orifice arrangement based on a fundamental difference between subsonic and supersonic pressure distributions.

4. The repeatability of aerodynamic-compensation performance was demonstrated by the close agreement of test results for different probes of the same design tested in different wind tunnels.

5. The performance of an aerodynamic-compensation probe was not greatly influenced by a gradual enlargement of the downstream portion of the probe or by incorporation of a total-pressure opening in the nose of the probe.

6. The performance of aerodynamic-compensation probes ahead of a slender-nose model was approximately that estimated, whereas the performance ahead of bluff-nose and intermediate-nose models was complicated by the severe pressure gradients. Proper compensation for error ahead of bluff-nose and intermediate-nose configurations can be obtained by making allowances for existing flow conditions.

7. The method for aerodynamic compensation for position error at subsonic and near-sonic speeds was successfully combined with methods for aerodynamic reduction of errors due to angle of attack.

LANGLEY RESEARCH CENTER,
NATIONAL AERONAUTICS AND SPACE ADMINISTRATION,
LANGLEY FIELD, VA., *February 25, 1959.*

REFERENCES

1. Larson, Terry J., Stillwell, Wendell H., and Armistead, Katharine H.: Static-Pressure Error Calibrations for Nose-Boom Airspeed Installations of 17 Airplanes. NACA RM H57A02, 1957.
2. Anon.: Standard Atmosphere—Tables and Data for Altitudes to 65,800 Feet. NACA Rep. 1235, 1955. (Supersedes NACA TN 3182.)
3. Werner, Frank D., and Geronime, Robert L.: Automatic Correction of Errors in Airplane Static Pressure Sources. WADC Tech. Rep. No. 56–193, U.S. Air Force, May 1956.
4. Bäuerle, H.: Measuring Instruments for Pressure, Velocity, and Direction Measurements. Reps. and Translations No. 951, British M.A.P. Völkenrode, Mar. 15, 1947.
5. Korkegi, Robert H.: An Aerodynamic Means of Static Pressure Compensation for Transonic and Supersonic Aircraft. Contract AF 33(616)-2396, Eng. Center, Univ. of Southern California, May 1956.
6. Korkegi, Robert H., and Mannes, Robert L.: Investigation of Free-Stream Pressure and Stagnation Pressure Measurement From Transonic and Supersonic Aircraft. WADC Tech. Rep. 55–238, U.S. Air Force, Mar. 1955.
7. Mannes, Robert L., and Stuart, Jay W., Jr.: Investigation of Free-Stream Pressure and Stagnation Pressure Measurement From Transonic and Supersonic Aircraft. Interim Phase Report II—Experimental. WADC Tech. Rep. 55–238, U.S. Air Force, July 1956.
8. Smetana, Frederick O., Stuart, Jay Wm., and Wilber, Paul C.: Investigation of Free-Stream Pressure and Stagnation Pressure Measurement From Transonic and Supersonic Aircraft. Interim Phase Report III—Development and Flight Test of Aerodynamic Static Pressure Compensation for a Service Type Aircraft. WADC Tech. Rep. 55–238, U.S. Air Force, July 1957.
9. O'Bryan, Thomas C., Danforth, Edward C. B., and Johnston, J. Ford: Error in Airspeed Measurement Due to the Static-Pressure Field Ahead of an Airplane at Transonic Speeds. NACA Rep. 1239, 1955. (Supersedes NACA RM L9C25 by Danforth and Johnston, RM L50L28 by Danforth and O'Bryan, and RM L52A17 by O'Bryan.)
10. Huston, Wilber B.: Accuracy of Airspeed Measurements and Flight Calibration Procedures. NACA Rep. 919, 1948. (Supersedes NACA TN 1605.)
11. Lindsey, W. F.: Effect of Mach Number on Position Error as Applied to a Pitot-Static Tube Located 0.55 Chord Ahead of an Airplane Wing. NACA WR L–75, 1944. (Formerly NACA CB L4E29.)

12. Wright, Ray H., Ritchie, Virgil S., and Pearson, Albin O.: Characteristics of the Langley 8-Foot Transonic Tunnel With Slotted Test Section. NACA Rep. 1389, 1958. (Supersedes NACA RM L51H10 by Wright and Ritchie and RM L51K14 by Ritchie and Pearson.)
13. Loving, Donald L., and Estabrooks, Bruce B.: Transonic-Wing Investigation in the Langley 8-Foot High-Speed Tunnel at High Subsonic Mach Numbers and at a Mach Number of 1.2. Analysis of Pressure Distribution of Wing-Fuselage Configuration Having a Wing of 45° Sweepback, Aspect Ratio 4, Taper Ratio 0.6, and NACA 65A006 Airfoil Section. NACA RM L51F07, 1951.
14. Estabrooks, Bruce B.: An Analysis of the Pressure Distribution Measured on a Body of Revolution at Transonic Speeds in the Slotted Test Section of the Langley 8-Foot Transonic Tunnel. NACA RM L52D21a, 1952.
15. Robinson, Harold L.: Pressures and Associated Aerodynamic and Load Characteristics for Two Bodies of Revolution at Transonic Speeds. NACA RM L53L28a, 1954.
16. Matthews, Clarence W.: A Comparison of the Experimental Subsonic Pressure Distributions About Several Bodies of Revolution With Pressure Distributions Computed by Means of the Linearized Theory. NACA Rep. 1155, 1953. (Supersedes NACA TN 2519.)
17. Cole, Richard I.: Pressure Distributions on Bodies of Revolution at Subsonic and Transonic Speeds. NACA RM L52D30, 1952.
18. Thompson, Jim Rogers: Measurements of the Drag and Pressure Distribution on a Body of Revolution Throughout Transition From Subsonic to Supersonic Speeds. NACA RM L9J27, 1950.
19. Mollo-Christensen, Erik L., Landahl, Marten T., and Martuccelli, John R.: A Short Static-Pressure Probe Independent of Mach Number. Jour. Aero. Sci. (Readers' Forum), vol. 24, no. 8, Aug. 1957, pp. 625–626.
20. Cooper, Morton, and Hamilton, Clyde V.: Orientation of Orifices on Bodies of Revolution for Determination of Stream Static Pressure at Supersonic Speeds. NACA TN 2592, 1952.
21. Ziegler, Norman G.: Wind-Tunnel Calibration of the Given High-Speed Pitot-Static Probe at Mach Numbers of 1.57 and 1.88. Aero Data Rep. 33, David W. Taylor Model Basin, Navy Dept., Sept. 1955.
22. Braslow, Albert L., and Knox, Eugene C.: Simplified Method for Determination of Critical Height of Distributed Roughness Particles for Boundary-Layer Transition at Mach Numbers From 0 to 5. NACA TN 4363, 1958.
23. Luther, Marvin: Fixing Boundary-Layer Transition on Supersonic Wind-Tunnel Models. Jour. Aero. Sci., vol. 24, no. 8, Aug. 1957, pp. 579–586.
24. Brunn, Cyril D., and Stillwell, Wendell H.: Mach Number Measurements and Calibrations During Flight at High Speeds and at High Altitudes Including Data for the D–558–II Research Airplane. NACA RM H55J18, 1956.
25. Pearson, Albin O., and Brown, Harold A.: Calibration of a Combined Pitot-Static Tube and Vane-Type Flow Angularity Indicator at Transonic Speeds and at Large Angles of Attack or Yaw. NACA RM L52F24, 1952.

U.S. GOVERNMENT PRINTING OFFICE: 1960